Biochemical and Biophysical Research Communications 452 (2014) 661–664

Contents lists available at ScienceDirect

Biochemical and Biophysical Research Communications

journal homepage: www.elsevier.com/locate/ybbrc

Vinculin E29R mutation changes cellular mechanics

Vera Auernheimer, Wolfgang H. Goldmann *

Department of Physics, Biophysics Group, Friedrich-Alexander-University of Erlangen-Nuremberg, 91052 Erlangen, Germany

ARTICLE INFO

Article history:
Received 19 August 2014
Available online 1 September 2014

Keywords:
Vinculin
Talin
F-actin
Focal adhesion
Mechanotransduction

ABSTRACT

We investigated the effect of the point mutation E29R on vinculin under cell mechanical aspects. MEFvcl KO cells were transfected with intact eGFP-vinculin (rescue) or mutant E29R vinculin. Cellular stiffness and adhesion strength of mutant E29R vinculin were considerably higher compared to rescue and MEFvcl KO cells. 2D traction microscopy also indicated markedly higher strain energy in E29R mutant cells compared to rescue and MEFvcl KO cells. Fluorescence recovery after photobleaching showed that the recovery time for mutant E29R cells was drastically slower than for MEFvcl rescue cells and that the mobile fraction was larger for rescue compared to E29R mutant cells. These results indicate that E29R mutation might prime the vinculin head for F-actin binding, which results in higher cell stiffness, contractile force, and strengthening of focal adhesions.

1. Introduction

Vinculin is a globular focal adhesion (FA) protein consisting of 5 helical domains, where D1–D4 together form the vinculin head (Vh), which is connected to the vinculin tail domain (Vt) by a flexible linker region [1,2]. When the head domain (D1) interacts with the tail domain, the molecule is considered to be in a closed conformation. The tail domain contains binding sites for F-actin, paxillin, and PIP_2, while the head domain, D1 holds binding sites for talin, alpha-actinin, and alpha-catenin. In the closed conformation, vinculin is unable to bind both filamentous actin at Vt and talin at D1. This conformation is also referred to as the auto-inhibited, inactive state. In the cytosol, vinculin adopts a default auto-inhibited conformation forming Vh and Vt intramolecular interactions.

Recently, Janssen et al. [3] proposed a model whereby F-actin binding to vinculin may weaken the interaction between the head and tail domain, which would increase the likelihood for talin (in cell–matrix interactions) or alpha-catenin (in cell–cell adhesions) to bind and fully activate vinculin [4]. According to these researchers, the D1 region of the vinculin head stericly clashes with F-actin that prevents the linkage between vinculin tail and F-actin.

Golji et al. [5] evaluated the impact of different vinculin head domain residues interacting with F-actin in molecular dynamics simulations. These researchers confirmed that D1 is separated from the vinculin tail in the open conformation, and found that the amino acids E28 and E29 are available for linking the vinculin head to the F-actin surface. They argued that the open conformation of vinculin facilitates the binding of vinculin with F-actin not only by removing the steric hindrance for vinculin tail-F-actin interaction, but also through contributing an additional binding interface between D1 and F-actin. Alternatively, the clash between vinculin head (D1) and F-actin, if coupled with stress transduced to vinculin through its connection with talin, could also catalyze the movement of the head away from vinculin tail [5]. Conformational changes leading to the opening of the vinculin molecule have been described in several combinatorial models [2,6,7].

In this study, we analyzed vinculin's role using the MEFvcl E29R variant in magnetic tweezer, 2D-traction microscopic, and fluorescence recovery after photobleaching (FRAP) experiments and compared the results with MEFvcl rescue and MEFvcl KO cells. Our findings suggest that vinculin activation, F-actin binding, and subsequent force transmission are associated with amino acid E29 of vinculin as well as increased stability of vinculin incorporation in focal adhesions.

2. Materials and methods

2.1. Cell culture

Mouse embryonic fibroblasts (MEF) wild-type (WT) and vinculin knock-out (KO) were obtained from Dr. W.H. Ziegler [8]. These cell lines were maintained in a low glucose (1 g/L) Dulbecco's modified Eagle medium (Life Technologies, Darmstadt, Germany) supplemented with 10% fetal calf serum (low endotoxin) and 2 mM L-glutamine kept at 37 °C with 5% CO_2. Mycoplasma contamination was excluded using a mycoplasma detection kit (Minerva Biolabs, Berlin, Germany).

* Corresponding author.
E-mail address: wgoldmann@biomed.uni-erlangen.de (W.H. Goldmann).

http://dx.doi.org/10.1016/j.bbrc.2014.08.133
0006-291X/

2.2. Cloning and expression of vinculin

Generation of the eukaryotic expression vector pcDNA3.1, including eGFP-tagged wild-type vinculin was previously described by [9]. The same cDNA vector was used to obtain the mutant. Using site-directed mutagenesis on position 29, glutamic acid (E) was replaced by arginine (R).

To create the point mutation, primers were ordered from MWG-Biotech (Eurofins MWG Operon, Ebersberg, Germany). Phusion High-Fidelity DNA Polymerase and the restriction enzyme DpnI for the digestion of methylated DNA were purchased from Cell Signaling (NEB, Frankfurt, Germany). DNA-vectors were amplified in *Escherichia coli* strain Dh5α and purified using the NucleoBond PC 500 kit (Macherey–Nagel, Düren, Germany). The complete sequence for the eGFP-tagged vinculin mutant was confirmed by sequencing (GATC Biotech AG, Konstanz, Germany). MEF cells (1.5×10^5) were seeded overnight in 35 mm cell culture dishes prior to transfection. Transfection was carried out in serum-free DMEM using 2 μg DNA and Lipofectamine 2000 (Invitrogen, Germany). The day after transfection, cells were re-seeded in 35 mm culture dishes or placed on PAA-traction gels, respectively.

2.3. Magnetic tweezer microrheology

We used a magnetic tweezer device as described by [10]. For measurements, $3–4 \times 10^4$ cells were seeded overnight into a 35 mm tissue culture dish. Thirty minutes before the experiment, the cells were incubated with fibronectin-coated paramagnetic beads of 4.5 μm Ø (Invitrogen, Karlsruhe, Germany). A magnetic field was generated using a solenoid with a needle-shaped core (HyMu80 alloy, Carpenter, Reading, PA). The needle tip was placed at a distance of 20–30 μm from a bead bound to the cell using a motorized micromanipulator (Injectman NI-2, Eppendorf, Hamburg, Germany). A staircase-like, increasing force was then applied for 10 s to the bead bound on the cell surface [11]. During measurements, bright-field images were taken by a CCD camera (ORCA ER, Hamamatsu) at a rate of 40 frames/s. The bead position was tracked on-line using an intensity-weighted center-of-mass algorithm. Measurements on multiple beads per well were performed at 37 °C for 0.5 h, using a heated microscope stage on an inverted microscope at 40× magnification (NA 0.6) under bright-field illumination. Transfected eGFP-positive MEF cells were identified in fluorescence mode.

2.4. 2D-traction microscopy

Different MEFs were plated overnight on fibronectin-coated polyacrylamide hydrogels (Young's modulus of 18,000 Pa) at 37 °C and 5% CO_2 in DMEM medium. Gels were prepared according to a modified protocol by Pelham and Wang [12]. Using cytochalasin D and trypsin, cells were detached and images were recorded before and after relaxation of the gel. Comparing the position of fluorescent microspheres in the deformed and undeformed states, the traction field was obtained using a difference-with-interpolation algorithm with a spatial resolution of 2.5 nm and an accuracy of 8 nm. Tractions were computed according to a Fourier-based-algorithm [13].

2.5. Fluorescence recovery after photobleaching (FRAP)

FRAP studies were performed with the confocal microscope (Leica) and a 20× dip-in objective inside the incubation chamber. Transfected cells were cultivated in 35 mm dishes the day before, and cells – expressing medium levels of eGFP-vinculin constructs and focal adhesions that showed no growth or disassembly – were chosen for measurements. A 488 nm argon laser was used for eGFP excitation and bleaching. Image acquisition started 1 min before bleaching and continued for 5 min of the recovery process (1 frame/4 s). FRAP movies were analyzed using ImageJ and Matlab software [14]. Intensities of the bleached focal adhesions as well as reference adhesions were corrected for background fluorescence, and the bleached area was normalized by the average reference adhesion signal. Every recovery curve was fitted with a single exponential function, and the mean value of all half-life recovery times ($t_{1/2}$) as well as the immobile fractions were calculated.

3. Results and discussion

Glutamic acid (E, negatively charged) on position 29 of the vinculin molecule was replaced by arginine (R, positively charged) to test the cellular mechanical changes induced by this point mutation. Both vinculin constructs, (full length vinculin = rescue) and

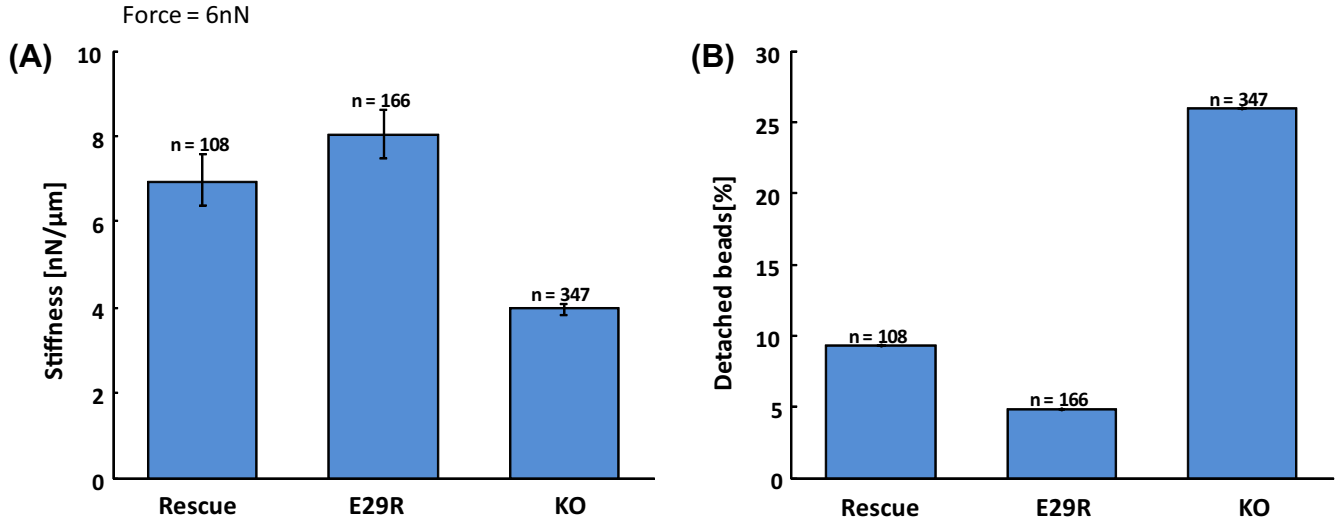

Fig. 1. (A) Magnetic tweezer measurements of MEFvcl rescue, MEFvcl E29R, and MEFvcl KO cells. All cells were incubated with fibronectin-coated paramagnetic beads (Ø 4.5 μm) for 30 min, after which the paramagnetic beads were displaced from their original position by force application of the magnetic tweezer. From the displacement, the cell stiffness was calculated at 6 nN force. The standard error of the mean (SEM) and the number of cells are indicated. (B) Binding (adhesion) strength of MEFvcl rescue, MEFvcl E29R, and MEFvcl KO cells are represented by the percentage of detached beads during measurements.

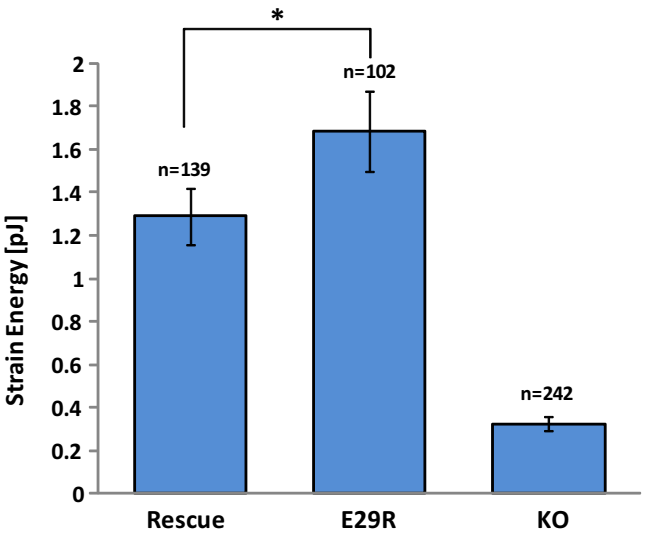

Fig. 2. 2D traction microscopy of MEFvcl rescue, MEFvcl E29R, and MEFvcl KO cells. All cells were seeded on fibronectin-coated elastic substrates (18 kPa), and tractions were determined. The strain energy values of MEFvcl rescue and MEFvcl E29R cells were between 4 and 6-fold higher than MEFvcl KO cells. The standard error of the mean (SEM) and the number of cells analyzed per cell line are indicated. The asterisk indicates a significance level of $^{*}p < 0.05$.

E29R mutant were expressed in MEFvcl KO cells, and the cell stiffness was measured. Using the magnetic tweezer device and applying up to 10 nN force on fibronectin-coated beads (mimicking the ECM) attached to integrins, we observed that the E29R mutant showed notably higher cell stiffness compared to rescue and vinculin-deficient (KO) cells (Fig. 1A). The binding (adhesion) strength of these cells was also determined by calculating the percentage of detached beads during measurements (Fig. 1B). Markedly fewer beads detached from the E29R mutant compared to rescue and MEFvcl KO cells. These results support the notion that the mutation of E29R might separate the head (D1) from the tail domain, and that the mutated vinculin is capable of linking to the F-actin surface [3]. Previous simulations have shown that vinculin facilitates the binding of vinculin with the actin filament not only by removing the steric hindrance of vinculin tail-F-actin interaction, but also through contributing an additional binding interface between D1 and F-actin [5].

Further support for this view comes also from two-dimensional traction force microscopy. The contractile forces generated *via* the intracellular integrin-FA-actomyosin link are significantly higher in mutant E29R compared to rescue and MEFvcl KO cells (Fig. 2). We, therefore, believe that changing the charge of the amino acid on position 29 of vinculin influences its force transmission function. Janssen et al. [3] proposed that actin binding to vinculin weakens the binding of the head region to the tail of vinculin and Wen et al. [15] recently suggested actin-vinculin binding triggers actin polymerization and that vinculin may act as an actin nucleation site in focal adhesions.

Since the dynamics of focal adhesion proteins are linked to focal adhesion assembly/disassembly and consequently to force generation [14], we also determined the exchange rates of vinculin in focal adhesions using the FRAP technique. The exchange rates of vinculin in focal adhesions were measured in MEFvcl KO cells re-expressing intact vinculin (=rescue) and in E29R vinculin mutant cells. The half-maximum recovery time after photobleaching ($t_{1/2}$) of vinculin fused with eGFP was quantified (Fig. 3A).

Vinculin half-life recovery time in MEFvcl rescue cells was $t_{1/2} = 67 \pm 8$ s, and in cells expressing the vinculin mutant E29R the exchange rate was noticeably slower ($t_{1/2} = 157 \pm 30$ s). These results indicate that the mutant E29R decreased the exchange dynamics in focal adhesions and increased the stability of vinculin incorporation, which is also indicated by the ratio of the mobile/immobile fraction of MEFvcl rescue and E29R mutant cells (Fig. 3B). The immobile fraction was higher in E29R mutant (42%) than in rescue cells (28%). These results imply that the changed electrical charge (E29 to R) of the vinculin head domain may weaken the interaction of the head/tail interaction and exposes the auto-inhibited form of vinculin to F-actin linkage to allow for higher force transduction.

Many studies have reported on the vinculin molecule being in the auto-inhibited, inactive state preventing the association

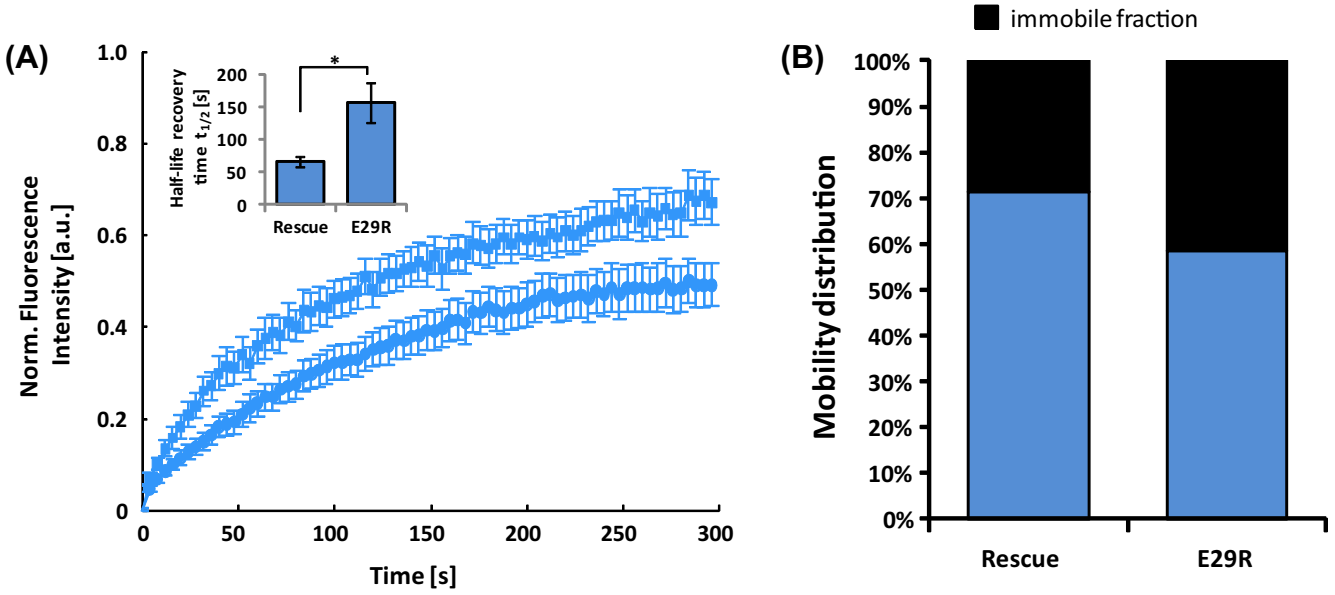

Fig. 3. Dynamics of vinculin variants measured by FRAP. (A) Fluorescence recovery curves of eGFP-fused vcl rescue and vcl E29R proteins in MEF cells. The bar plot (inset) shows the mean half-life recovery times with standard error of the mean (SEM). The number of cells analyzed per cell line was $n \geqslant 21$. The asterisk indicates a significance level of $^{*}p < 0.05$. (B) Plot of the portion (%) of the mobile/immobile fraction of vinculin variants in focal adhesions. Mobile fractions are indicated in blue, and immobile fractions are presented in black. (For interpretation of the references to color in this figure legend, the reader is referred to the web version of this article.)

between vinculin tail and F-actin in the cytosol of cells. Janssen et al. [3] addressed the interaction of F-actin with the vinculin head. They suggested two patches of basic residues on the surface of vinculin link with two patches of acidic residues on the surface of F-actin. Golji et al. [5] predicted from simulations that amino acids on position 28 and 29 of vinculin are likely candidates for linking with the F-actin surface. It is, however, still unclear how steric clashes between the head domain D1 and F-actin prevent binding, and which of the acidic patches on F-actin are critical to associate with vinculin.

Vinculin-actin binding is also necessary for focal adhesions to be mechanically resilient, and the interaction is crucial for strengthening focal adhesions (Figs. 1 and 2). Recent findings describe vinculin as a major regulator of focal adhesions [16,17]. In cells, low-affinity interactions of vinculin with talin in initial adhesion complexes at the leading edge keep vinculin in place for possible associations with PIP_2 or actin, which subsequently leads to its activation [1–3,18,19]. If vinculin does not become activated at this stage, adhesion complexes turn over rapidly, thus when activated, it stabilizes the active conformation of focal adhesions, resulting in reduced focal adhesion turnover (Fig. 3A and B).

Acknowledgments

We thank Drs. Gerold Diez and James Smith for technical help and Drs. Ingo Thievessen and Ben Fabry for stimulating discussions. This work was supported by grants from Deutscher Akademischer Austausch Dienst and Deutsche Forschungsgemeinschaft.

References

[1] C. Bakolitsa, J.M. de Pereda, C.R. Bagshaw, D.R. Critchley, R.C. Liddington, Crystal structure of the vinculin tail suggests a pathway for activation, Cell 99 (1999) 603–613.
[2] C. Bakolitsa, D.M. Cohen, L.A. Bankston, A.A. Bobkov, G.W. Cadwell, L. Jennings, D.R. Critchley, S.W. Craig, R.C. Liddington, Structural basis for vinculin activation at sites of cell adhesion, Nature 430 (2004) 583–586.
[3] M.E. Janssen, E. Kim, H. Liu, L.M. Fujimoto, A. Bobkov, N. Volkmann, D. Hanein, Three-dimensional structure of vinculin bound to actin filaments, Mol. Cell 21 (2006) 271–281.
[4] D.M. Cohen, H. Chen, R.P. Johnson, B. Choudhury, S.W. Craig, Two distinct head-tail interfaces cooperate to suppress activation of vinculin by talin, J. Biol. Chem. 280 (2005) 17109–17117.
[5] J. Golji, M.R. Mofrad, The interaction of vinculin with actin, PLoS Comput. Biol. 9 (2013) e1002995.
[6] H. Chen, D.M. Choudhury, S.W. Craig, Coincidence of actin filaments and talin is required to activate vinculin, J. Biol. Chem. 281 (2006) 40389–40398.
[7] W.H. Goldmann, V. Auernheimer, I. Thievessen, B. Fabry, Vinculin, cell mechanics, and tumor cell invasion, Cell Biol. Int. 37 (2013) 397–405.
[8] C.T. Mierke, P. Kollmannsberger, D.P. Zitterbart, G. Diez, T.M. Koch, S. Marg, W.H. Ziegler, W.H. Goldmann, B. Fabry, Vinculin facilitates cell invasion into three-dimensional collagen matrices, J. Biol. Chem. 285 (2010) 13121–13130.
[9] G. Diez, V. Auernheimer, B. Fabry, W.H. Goldmann, Head/tail interaction of vinculin influences cell mechanical behavior, Biochem. Biophys. Res. Commun. 406 (2011) 85–88.
[10] P. Kollmannsberger, B. Fabry, Linear and nonlinear rheology of living cells, Annu. Rev. Mater. Res. 41 (2011) 75–97.
[11] N. Bonakdar, J. Luczak, L. Lautscham, M. Czonstke, T.M. Koch, A. Mainka, T. Jungbauer, W.H. Goldmann, R. Schröder, B. Fabry, Biomechanical characterization of a desminopathy in primary human myoblasts, Biochem. Biophys. Res. Commun. 419 (2012) 703–707.
[12] R.J. Pelham Jr., Y. Wang, Cell locomotion and focal adhesions are regulated by substrate flexibility, Proc. Natl. Acad. Sci. U.S.A. 94 (1997) 13661–13665.
[13] J.P. Butler, I.M. Tolic-Norrelykke, B. Fabry, J.J. Fredberg, Traction fields, moments, and strain energy that cells exert on their surroundings, Am. J. Physiol. Cell Physiol. 282 (2002) C595–C605.
[14] K. Küpper, N. Lang, C. Möhl, N. Kirchgessner, S. Born, W.H. Goldmann, R. Merkel, B. Hoffmann, Tyrosine phosphorylation of vinculin at position 1065 modifies focal adhesion dynamics and cell tractions, Biochem. Biophys. Res. Commun. 399 (2010) 560–564.
[15] Q. Wen, P.A. Janmey, Polymer physics of the cytoskeleton, Curr. Opin. Solid State Mater. Sci. 15 (2011) 177–182.
[16] C. Grashoff, B.D. Hoffman, M.D. Brenner, R. Zhou, M. Parsons, M.T. Yang, M.A. McLean, S.G. Sligar, C.S. Chen, T. Ha, M.A. Schwartz, Measuring mechanical tension across vinculin reveals regulation of focal adhesion dynamics, Nat. Lett. 466 (2010) 263–267.
[17] I. Thievessen, P.M. Thompson, S. Berlemont, K.M. Plevock, S.V. Plotnikov, A. Zemljic-Harpf, R.S. Ross, M.W. Davidson, G. Danuser, S.L. Campbell, C.M. Waterman, Vinculin–actin interaction couples actin retrograde flow to focal adhesions, but is dispensable for focal adhesion growth, J. Cell Biol. 202 (2013) 163–177.
[18] S. Hüttelmaier, O. Mayboroda, B. Harbeck, T. Jarchau, B.M. Jockusch, M. Rüdiger, The interaction of the cell-contact proteins VASP and vinculin is regulated by phosphatidylinositol-4,5-bisphosphate, Curr. Biol. 8 (1998) 479–488.
[19] Y. Chen, N.V. Dokholyan, Insights into allosteric control of vinculin function from its large scale conformational dynamics, J. Biol. Chem. 281 (2006) 29148–29154.